Egyptian Journal of Chemistry

http://ejchem.journals.ekb.eg/

Nickel hydroxide/polystyrene composites for adsorptive removal of Fe (III) and methylene blue from aqueous solutions

Ahmed Bakry[a]*, Marzouk Adel[b], Ahmed M. A. El Naggar[c], Maher Helmy Helal[a]

[a]*Chemistry Department, Faculty of Science, Hewlan University, 11795-Cairo, Egypt*
[b]*Aluminum Sulphate Co. of Egypt (ASCE)*
[c]*Egyptian Petroleum Research Institute (EPRI), Nasr City, Cairo- Egypt*

Abstract

Removal of industrial dyes and metals into water has been considered as a serious environmental problem. To solve this issue, in this study nickel hydroxide/polystyrene composites adsorbents were introduced for the water remediation from the harmful methylene blue dye and Fe (III). Polystyrene was obtained from its monomers using emulsion polymerization technique. The composite was obtained by precipitating nickel hydroxide from its solution on polymer surface by enhancing pH of the medium. The structural and morphological characteristics of the synthesized composites were investigated by Fourier transform infrared (FTIR) spectroscopy, scanning electron microscopy (SEM), energetic dispersive X-ray (EDX), and x-ray diffraction (XRD). FT-IR spectra for composites showed the characteristic peaks of polystyrene and that correspond to hydroxide from $NiOH_2$ (3442 cm^{-1}). SEM analysis showed that the $Ni(OH)_2$ were distributed on the surface of polystyrene in a regular manner. EDX analysis showed the presence of 19.9 wt% of Ni on the composite. XRD analysis showed the characteristic diffraction peaks at 2θ = 19.54 corresponding to polystyrene and at 2θ = 32.5, 38.5, 52.1, and 58.97 corresponds to $Ni(OH)_2$. The composite was tested as an adsorbent using the batch technique. The impact of solution pH, contact time, and absorbent dose on the adsorption processes were studied to optimize the operational parameters. Kinetic and equilibrium studies showed that the adsorption processes followed pseudo-first-order kinetic and Freundlich isotherm. Maximum adsorption capacities of 32.73 and 58.24 mg g^{-1} were achieved in case of MB and Fe (III), respectively. Thermodynamic studies showed that ΔG values for the adsorption processes ranged from -0.075 to -1.435 kJ mol^{-1} by changing temperature from 303K to 343 in case of MB; ΔG values ranged from -0.467 to -1.548 kJ mol^{-1} by changing temperature from 303K to 343 in case of Fe (III). Negative values ΔG revealed that the adsorption processes were spontaneous and feasible. Hence, nickel hydroxide/PS composites could be potentially used for treating wastewater from MB and Fe (III).

Adsorption; Composites; Metal hydroxide; Wastewater; Polystyrene; Methylen blue; Iron

1. Introduction

The excessive industrial, agricultural, and regional activities throughout the world have resulted in huge amounts of wastewater. There are mainly three types of contaminants exists in the wastewater, namely, microorganisms, organics, and inorganics [1]. Major parts of organic and inorganic pollutants are dyes and metal ions, respectively. These contaminants have gained lots of interest because of their toxicities to ecological and biological systems [2]. The metal pollutants such as iron, cadmium and lead have resulted from many industries including fertilizer industries, metal plating, mining operations, paper industries and pesticides. The dye contaminants such as methylene blue, reactive dyes and methyl orange result from pharmaceuticals, cosmetics, leather, textile, plastic, and paper industries [3], [4].

These pollutants have attracted special concerns because of the ability of organisms to store, accumulate and transfer them. This can result in severe public health problems to animals and human beings [5]. Accordingly, wastewater systems have become an important problem which urgently should be solved. An enormous amount of work has been reported about dealing with the water pollution due to dyes and metal ions. The developed methods to

*Corresponding author e-mail: ahmed.bakry@science.helwan.edu.eg; (Ahmed Bakry).
Receive Date: 25 November 2021, **Revise Date:** 12 December 2021, **Accept Date:** 16 December 2021
DOI: 10.21608/EJCHEM.2021.105565.4937

circumvent water pollution include osmosis [6], adsorption [7], electrochemical precipitation [8], ion exchange [9] and flocculation [10]. Among these techniques, adsorption is extensively used to remove metal ions and dyes from wastewater. This is because the adsorption process offers the simplicity, low cost, and the high efficiency [11]. Experimented adsorbents include zeolites, polymers, biomass, carbon materials, metal oxides and clays [12].

Polymers are characterized by many good features including tolerability [13], good mechanical properties [14], processability [15], and low cost [16]. Hence, polymers are employed widely for many applications such as packaging [17], tissue engineering [18], [19], drug delivery [20] and wastewater remediation [4]. Polymer composites can offer superior properties over single polymers for specific applications including transportation, marine, aerospace/defense, electromagnetic shielding and wastewater treatment [21]–[23]. The adsorption efficiency of polymer composite toward pollutants present in water was studied extensively. [24] Among experimented composites are metal−organic framework/polydopamine composite [25] and clay based composites [26]. Metal oxides and metal hydroxides offer unique physical and chemical properties such as high specific surface areas and abundant active sites. Hence, they have been used for many applications including catalysis and water treatment [27]. However, their high-surface to-volume ratio increases their tendency to aggregate. Nevertheless, combining polymers with metal oxides and metal hydroxides in composites can avoid this effect and results in a hybrid polymeric/inorganic materials exhibiting properties cannot be are not presented by separate materials [21]. For instance, polypyrrole nanofiber/Zn-Fe layered double hydroxide composites were prepared for the removal of safranin dye from aqueous solutions [28].

Accordingly, the present study investigates the ability to use nickel hydroxide/polystyrene composites for the removal of methylene blue and iron from aqueous solutions. The composite was simply prepared by precipitating of nickel hydroxide from its precursors in the aqueous medium on the surface of PS surface at basic pH. The physiochemical properties of the obtained composites were characterized by diverse techniques including FT-IR, SEM-EDX and XRD. The dependence of the adsorption processes on the operational parameters including pH of the medium, composite dose and contact time were investigated. Adsorption isotherm and thermodynamics of the adsorption processes were also studied.

2. Experimental

2.1. Materials

Styrene, potassium per sulfate, sodium dodecyl sulfate, and ferric chloride were bought from Al-Gomhoria Company for Pharmaceuticals and Chemical Industries (Egypt). The reagents were used as received. Methylene blue dye were purchased from Sigma-Aldrich Co. (St Louis, MO, USA)

2.2. Preparation of PS

Polystyrene was synthesized via emulsion polymerization technique. Styrene (4.96 g) was mixed with sodium dodecyl sulfate (0.494 g) surfactant. The mixture was added to 11 ml of deionized water at 60°C under stirring. Potassium per sulfate (0.23 g) was added to the mixture. The mixture was kept for 2 hours at 60°C with stirring. The emulsion was dried in an oven at 60°C for 12 hours to get the polymer.

2.3. Preparation of Ni(OH)2/PS composite

An aqueous solution of $NiCl_2$ was prepared (2.78 g in 213 mL deionized water) and kept under vigorous stirring at 90 ºC. To the resultant clear solution, PS particles (1.0 g) were added. After 15 minutes, NaOH (0.1 M) was added drop wise under stirring till complete precipitation of nickel hydroxide (pH of 10 – 11) on the surface of PS particles. The hot mixture was filtrated and washed several times with deionized water. The nickel hydroxide loaded polystyrene ($Ni(OH)_2$/PS) was then left to dry in an oven at 60 ºC.

2.4. Characterization of Ni(OH)2/PS composite

FT-IR analyses for PS and $Ni(OH)_2$/PS composite were conducted on a Perkin-Elmer Spectrometer 400 (PerkinElmer Inc., Waltham, MA, USA) equipped with a Golden Gate diamond single reflection device. The measurements were carried out in the region of 4000–400 cm^{-1} and at a resolution of 2 cm^{-1}. SEM images for the composite were acquired by SEM, QUANTA FEG 250, USA equipped with EDX analyzer. The specific area of the composite was measured by Quantachrome TouchWin™ version 1.21 instrument. The N_2 adsorption measurements were done at 77.35 K. X-ray diffraction patterns for the samples were obtained using Panalytical Diffractometer (X'Pert Pro, USA).

2.5. Adsorption studies

Adsorption studies were carried out using batch technique to investigate the adsorption behavior of MB and Fe (III) on $Ni(OH)_2$/PS composites. Stock solutions of Fe (III) (500 mg L^{-1}) and MB dye (100 mg L^{-1}) in distilled water were prepared. Further adsorbate solutions exhibiting other concentrations

were prepared through suitable dilution. The impacts of experimental parameters including the dose of the composite, pH of the adsorbate solution, time of contact, initial adsorbate concentration, and temperature on the adsorption efficiency of $Ni(OH)_2$/PS composites were investigated. The adsorption experiments were done by stirring the composite/adsorbate mixture (150 rpm) for definite periods. The adsorption experiments were performed by a composite dose of 1 g L^{-1}, 20 mL adsorbate solution (MB: 40 mg L^{-1} ; Fe^{+3}: 100 mg L^{-1}) of neutral pH (≈ 6.5), at 23±2°C. Specific conditions were utilized to follow the impact of the composite dose (0.5 to 5 g L^{-1}), contact time (10 to 250 minutes), pH (2 to 14), and temperature (23 to 70°C) on the adsorption processes. For equilibrium studies, different initial concentrations of MB (10-40 mg L^{-1}) and Fe^{+3} (100-200 mg L^{-1}) with a constant composite dose (1 g L^{-1}) were employed. After each adsorption experiment, the composite particles were separated from the adsorbate solution using a 0.45μm membrane. The first 4 mL were neglected, and then the absorbance of non-adsorbed MB solution was determined by an UV−visible spectrophotometer (Jasco V-550, Japan) at 663 nm. The concentration of MB solution was determined using a calibration curve previously constructed through utilizing various solutions of MB with known initial concentrations. The concentration of iron in the aqueous solution was determined utilizing Perkin-Elmer flame atomic absorption spectrophotometer-3100 (AAS).

The removal efficiency (R, %) of MB and Fe (III) on the $Ni(OH)_2$/PS composites and the adsorption capacity (q_e) were calculated using Eq. 1 and Eq. 2, respectively.

$$R\ (\%) = 100\ x\ (\frac{C_o - C_e}{C_o}) \qquad (1)$$

$$q_e = (C_o - C_e)\ x\ \frac{V}{m} \qquad (2)$$

where C_o is the initial concentration of the solution of the adsorbate (mg L^{-1}), C_e (mg L^{-1}) and q_e (mg g^{-1}) are the residual concentration of the adsorbate at equilibrium and the quantity of adsorbate that adsorbed on the composites, respectively. V (L) is the volume of the solution of the adsorbate utilized for the adsorption experiment, and m (g) is the mass of the adsorbent.

3. Results and discussion

3.1. Properties of Ni(OH)2/PS Composite

FT-IR spectra for PS prepared by emulsion polymerization and $Ni(OH)_2$/PS composite are shown in Fig. 1. Both spectra exhibit the characteristic peaks for PS structure. The peaks appeared at 3026 cm^{-1}, 2917 cm^{-1} and 2851 cm^{-1} correspond to H–C–H stretching vibration; 1735 cm^{-1} corresponds to –CH aromatic bending; 1596 cm^{-1} corresponds to C=C of the aromatic ring; 1485 cm^{-1} assigns to C–H out of plane or in plane bending vibration; 1451.5 cm^{-1} corresponds to deformation CH_2 + C=C of the aromatic ring; 1046 cm^{-1} corresponds to phenyl C–H in plane bending vibration; 751.5 and 696.8 cm^{-1} correspond to C=C bending [29]. These peaks proved that the styrene reacted during the emulsion polymerization reactions producing polystyrene. The spectrum of the $Ni(OH)_2$/PS composite showed a new intense broad strong absorption band centered at 3442 cm^{-1}. This band could be attributed to the –OH stretching vibration in nickel hydroxide present in the composite.

The morphology of $Ni(OH)_2$/PS composite, studied by SEM analysis, is introduced in Fig. 2. The $Ni(OH)_2$ particles were clearly observed on the surface of PS. The metal hydroxide particles tended to distribute in a good manner throughout the surface of PS.

To determine the elemental composition of $Ni(OH)_2$/PS composites, the elemental analysis was carried out by energy-dispersive X-ray spectroscopy (EDX) (Fig. 3). The EDX analysis exhibited the existence of Ni on the surface of PS. The results of the elemental analysis are shown in the inset of Fig. 3.

The results of X-ray diffraction (XRD), performed on the $Ni(OH)_2$/PS composites, is shown in Fig. 4. The diffraction peak centered at 2θ = 19.54, corresponds to the crystalline regions in polystyrene. The broadness of this peak, relative to other ones, could be attributed to the existence of ordered domains in the polymeric materials exhibiting different inter-planar distances causing diffraction peaks at different angles. Hence, the observed peak was resulted from a superposition of the individual peaks. The diffraction peaks observed at 2θ = 32.5, 38.5, 52.10 and 58.97 are assigned to $Ni(OH)_2$ [30]. The appearance of the significant crystal structure for $Ni(OH)_2$ in the XRD pattern confirmed the precipitation of the metal hydroxide on the polymer surface.

The specific surface area of the particles of $Ni(OH)_2$/PS composite was determined by adsorption of N_2. The adsorption isotherm was analyzed by using the Brunnauer, Emmett and Teller (BET) equation (Eq. (1).[31]

$$\frac{1}{V[(\frac{P_0}{P})-1]} = \frac{1}{V_m C} + \frac{(C-1)}{V_m C}\frac{P}{P_0} \qquad (3)$$

where P_0 is the initial pressure, P is the instant pressure, V is the total volume of gas (corrected to STP) adsorbed at pressure P, V_m is the volume of monolayer, the volume of gas required to cover the

whole surface of the solid with a unimolecular layer in $cm^3\ g^{-1}$ (corrected to STP), $C=\exp[(\Delta H_L-\Delta H_1)/RT]$, C is a constant, indicating the ratio between the adsorbed time of the molecules in the first layer and the adsorbed molecules in the second and subsequent layers. ΔH_L is the enthalpy of liquefaction and ΔH_1 is the enthalpy of adsorption of the first layer. The plot of $1/[V(P_0/P-1)]$ against P/P_0 yields a straight line of slope $[(C-1)/V_mC]$ and intercept $[1/V_mC]$, from which both V_m and C could be calculated.

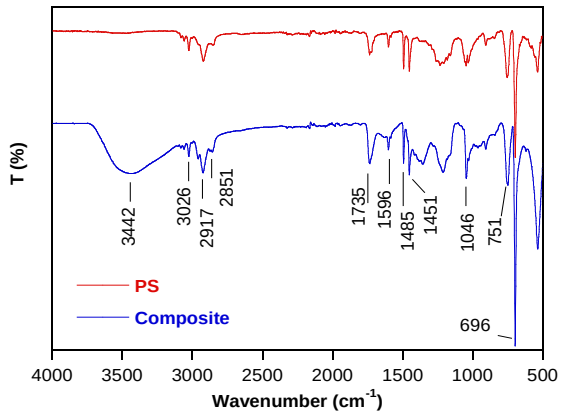

Fig. 1. FT-IR spectra for PS and $Ni(OH)_2$/PS.

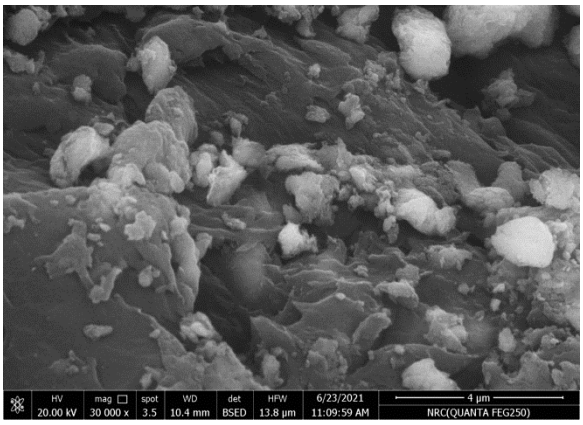

Fig. 2 SEM image of Ni(OH)2/PS composite.

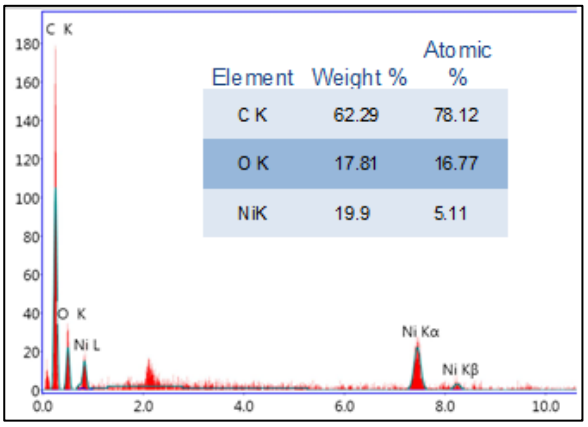

Fig. 3 EDX spectra of Ni(OH)2/PS

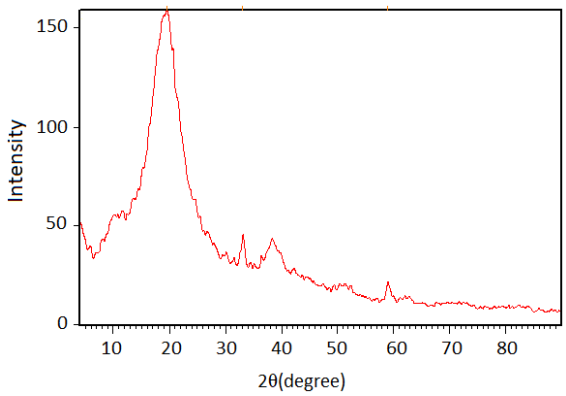

Fig. 4. XRD pattern of the $Ni(OH)_2$/PS composite.

Fig. 5 gives a plot of $1/[V(P_0/P-1)]$ against P/P_0, which was resulted from N_2 adsorption measurements for the particles of $Ni(OH)_2$/PS composite. The experimental data fitted on a straight line and exhibited a correlation coefficient of 0.999. In addition, the particles of $Ni(OH)_2$/PS composite exhibited high specific area of 42.91 $m^2\ g^{-1}$. This result reveals that $Ni(OH)_2$/PS composites could offer many adsorbing sites for up taking the adsorbate.

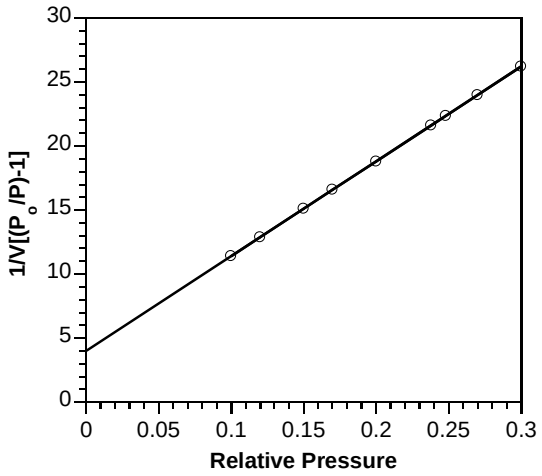

Fig. 5 BET plot for $Ni(OH)_2$/PS composite.

3.2. Influence of operational parameters in the adsorption process

3.2.1 Influence of pH

The pH of the medium of the adsorbate affects the surface charges on the adsorbent, and thus can affect the adsorption capacity of the adsorbent. Fig. 6a illustrates the change in the removal efficiency of the Fe (III) and MB solutions from Fe (III) and MB using the $Ni(OH)_2$/PS composite, with the change in the initial pH of the medium. Diverse effects of pH on the removal efficiency were observed for the two solutions. In the case of MB, the adsorption was lower in strong acidic or basic mediums with respect

to other mediums (pH 4-7). A similar observation has been reported before. [32] This behavior could be attributed the amphoteric nature of metal hydroxides which resulted in the solubility of metal hydroxides in strong acids or bases. Hence, further adsorption experiments were carried out at neutral pH (6.5).

In case of Fe (III) solutions, the *R* (%) tended to increase continuously with increasing pH. The effect of the amphoteric nature of the metal hydroxide loaded on PS was not observed in this case. This because as pH increased above 8, it was noted that Fe (III) separated from the medium as a brown precipitate (iron hydroxide). This mainly contributed to the continuous iron separation from the aqueous mediums with increasing the pH of the medium. Hence, to study the efficiency of $Ni(OH)_2$/PS composite to adsorb Fe (III), aside from the precipitation effects, the further adsorption experiments were done at neutral pH 6.5.

3.2.2 Influence of composite dose

The effects of composite dose (0.5 - 5 g L-1) on the removal of Fe (III) and MB from aqueous solutions are shown in Fig. 6b. A notable increase in the R% was observed as the dose of the adsorbent increased. This could be explained by the increase in the number of active sites available for adsorbing the adsorbate by increasing the adsorbent dose. About 87% of MB and 84% Fe (III) could be removed by using a dose of 4 g composite per liter. Further increase in the dose of the composite did not bring about an increase in the removal of MB or Fe (III).

3.2.3 Influence of contact time

Investigating the influence of contact time on the adsorption can help understand the relation between fixed quantities of the adsorbent and contact time as well as the adsorption−desorption equilibrium during contact time. The variations in *R* (%) with contact time (10-250 min) were studied at a fixed dose the of adsorbent (1 g L^{-1}), and the results are introduced in Fig. 6c. The adsorption occurred rapidly in the first period from 10 -150 relative to the periods above 150 min. Removal of about 55% of the dye and 58% of Fe (III) was achieved at contacting time of 150 min. The adsorption started rapidly at first due to the high availability of the adsorbing sites on the surface. Once most of these sites were occupied by the adsorbate molecules, the adsorption process tended to be slow.

3.3. Kinetics of adsorption

Investigating the kinetics of the adsorption process allow determining the rate and mechanism of the adsorption. The pseudo-first-order (Eq. 4),[33] and pseudo-second order (Eq. 5) [34] were applied on experimental results of adsorption, to find the best model that can describe the kinetics of the adsorption processes.

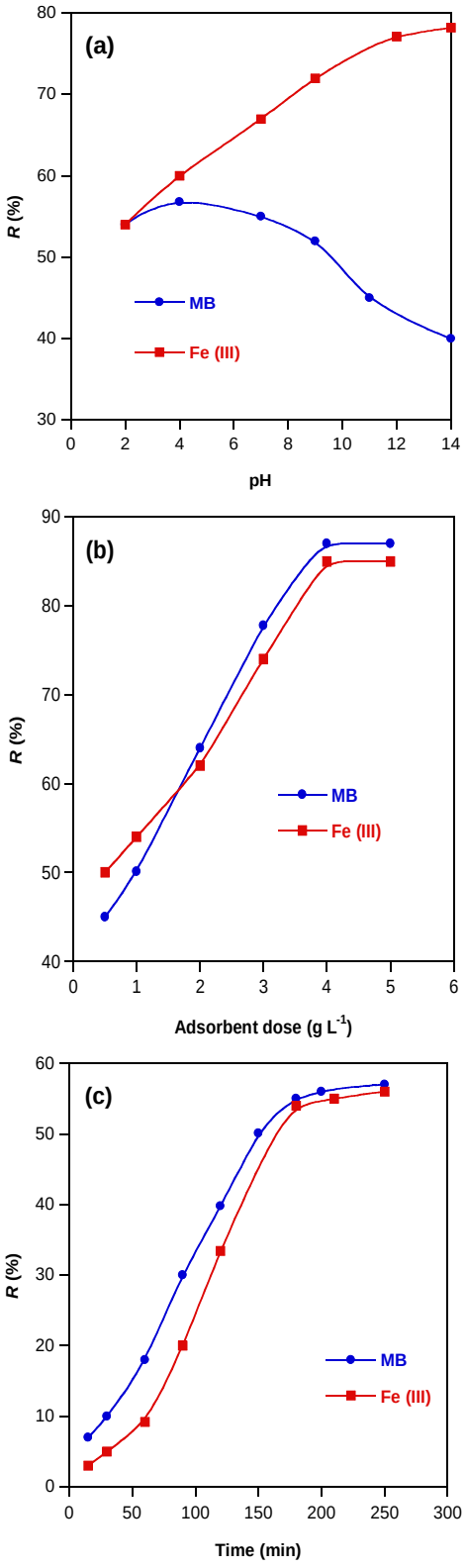

Fig. 6 Effect of operational parameters on removal efficiency (*R*, %) of $Ni(OH)_2$/PS composite: (a) effect of

pH, (b) effect of adsorbent dose and (c) effect of contact time.

$$\log(q_e - q_t) = \log(q_e) - \left(\frac{k_1}{2.303}\right) t \quad (4)$$

$$\frac{t}{q_t} = \frac{1}{k_2 q_e^2} + \frac{1}{q_e}\, t \quad (5)$$

where q_e and q_t are the adsorption capacities (mg g^{-1}) at equilibrium and at time t, respectively; k_1 (min^{-1}) and k_2 (g mg^{-1} min^{-1}) are the adsorption rate constants for the pseudo-first-order and pseudo-second-order. If the pseudo-first-order kinetic model fits the experimental data of adsorption, Eq. (4), then plotting log (q_e-q_t) versus t is expected to result in a straight line. This plot is useful to determine theoretical q_e and k from its intercept (log q_e) and slope (- k_1/2.303), respectively. However, in case the pseudo-second-order model, Eq. (5), can fit the adsorption, then plotting ($\frac{t}{q_t}$) as a function of time (t) will result in a straight line. This line allows evaluating the theoretical q_e and k_2 from the slope ($\frac{1}{q_e}$) and the intercept ($\frac{1}{k_2 q_e^2}$), respectively. The fitting of the adsorption data for MB and Fe (III) on $Ni(OH)_2$/PS composite with the models of kinetics is introduced in Figure 7. The estimated parameters for such models and the corresponding correlation coefficients (R^2) are given in Table 1. The pseudo-first-order kinetic model (Fig. 7a) seems to fit the experimental data of the adsorption of MB and Fe (III) on $Ni(OH)_2$/PS composite much better than the pseudo-second-order model (Fig. 7b). This was deduced form the higher value of R^2 observed for the pseudo-first-order model than that noted in case of the pseudo-second-order (Table 1). Moreover, the adsorption capacity calculated from the pseudo-first-order model ($q_{e,cal}$) was very close to the experimental one ($q_{e,exp}$) in contrary to that evaluated using the pseudo-second-order model.

TABLE 1 Adsorption kinetics parameters of MB and Fe (III) on $Ni(OH)_2$/PS composites.

		Adsorbate	
		MB	Fe (III)
Kinetic Model	$q_{e,exp}$ (mg g^{-1})	20.45	53.7
	Parameters		
pseudo-first-order	$q_{e,cal}$ (mg g^{-1})	20.77	53.26
	k_1 (min^{-1})	1.9x10^{-3}	6.1x10^{-4}
	R^2	0.9981	0.9531
pseudo-second-order	$q_{e,cal}$ (mg g^{-1})	43.923	44.64
	k_2 (g $mg^{-1}min^{-1}$)	5.18x10^{-5}	7.01x10^{-5}
	R^2	0.8106	0.7923

3.4. Adsorption isotherms

The adsorption isotherms describe the equilibrium of the adsorption process. These isotherms give the correlation between the adsorbate concentration at equilibrium and its quantity taken by the adsorbent at a specific temperature. Langmuir and Freundlich adsorption isotherms given in Eq. 6 and Eq. 7, respectively [35]. were employed to study the adsorption equilibrium.

$$\frac{C_e}{q_e} = \frac{1}{k_L q_{max}} + \frac{1}{q_{max}}\, C_e \quad (6)$$

$$\ln q_e = \ln K_F + \frac{1}{n}\, \ln C_e \quad (7)$$

where C_e (mg L^{-1}) and q_e (mg g^{-1}) are the concentration of residual adsorbate and that adsorbed at the equilibrium, respectively; q_{max} gives the maximum adsorption capacity of the composite; K_L represents the Langmuir constant which describe the adsorption energy and accessibility of the attaching positions on the composite (L mg^{-1}); n and K_F [mg g^{-1} (L $mg^{-1})^n$] represent the constants in the Freundlich isotherm which describe the intensity and capacity of the adsorption, respectively.

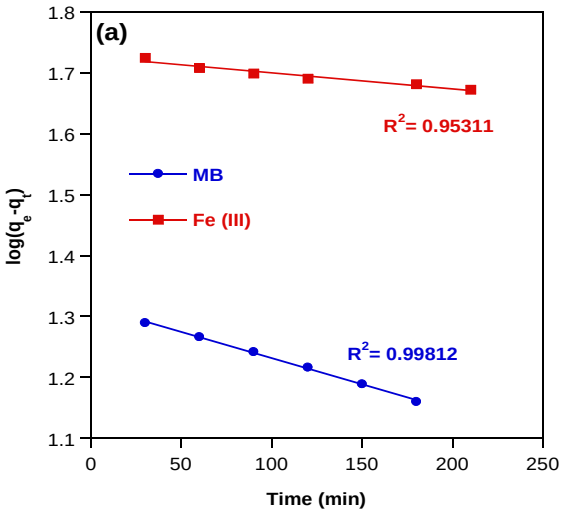

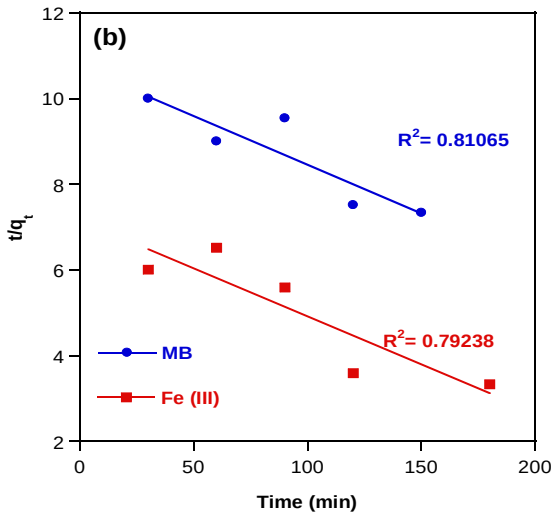

Fig. 7 Kinetic fits for adsorption of MB and Fe (III) on $Ni(OH)_2$/PS composites using different kinetic models: (a) pseudo-first-order; (b) pseudo-second-order

For the adsorption processes that follow Langmuir isotherm (Eq. 6), plotting ($\frac{C_e}{q_e}$) versus C_e gives a straight line. The slope and intercept of this line can be utilized to deduce both q_{max} and k_L, respectively. For adsorption processes that fit with Freundlich adsorption isotherm (Eq. 7), plotting (ln q_e) versus (ln C_e) results in a straight line. The values of K_F and n can be then evaluated from the intercept and slope of such line, respectively. The Langmuir model deals with adsorbents exhibiting homogeneous distribution of binding sites which have a similar tendency to adsorb a monolayer from the adsorbate. This model is useful to evaluate the maximum adsorption capacity of the adsorbent. Freundlich adsorption isotherm describes adsorbents attaining heterogeneous distribution of the binding sites which exhibit different tendencies toward the adsorbate. This model describes multilayer formation of the adsorbate on the surface of the adsorbent [36].

Fitting the experimental findings of the adsorption processes using various initial concentrations of the adsorbates with the adsorption isotherms is illustrated in Figure 8. The deduced model parameters are summarized in Table 2. The regression coefficients (R^2) observed for Freundlich adsorption isotherm are higher than those observed for Langmuir isotherm. This reveals that the Freundlich adsorption isotherm is the most suitable model to describe the adsorption of MB and Fe (III) on $Ni(OH)_2$/PS composites. The values of maximum adsorption capacity (q_{max}) given in Table 2 reveal that the $Ni(OH)_2$/PS composites can efficiently remove such pollutants from wastewater.

Table 2. The parameters of Freundlich and Langmuir isotherm models.

Isotherm Models	Model Parameters	Adsorbent	
		MB	Fe (III)
Langmuir isotherm	q_{max} (mg g^{-1})	32.73	58.24
	K_L (L mg^{-1})	0.066	0.115
	R^2	0.649	0.947
Freundlich isotherm	K_F [mg g^{-1} (L $mg^{-1})^n$]	2.31	4.08
	$1/n$	0.72	0.69
	R^2	0.981	0.978

3.5. Thermodynamics studies

The effect of temperature increasing on the adsorption of MB and Fe (III) on $Ni(OH)_2$/PS composites is shown in Fig. 10a. The removal efficiency tended to increase with temperature increase. This means that the rise in temperature favored the adsorption process, and thus the adsorption processes were endothermic. The thermodynamic parameters including enthalpy change (ΔH), entropy change (ΔS) and free energy (ΔG) for the adsorption processes were deduced using Eqs. 8-10.

$$K_d = \frac{q_e}{c_e} \quad (8)$$

$$lnK_d = \frac{\Delta S}{R} - \frac{\Delta H}{R}\frac{1}{T} \quad (9)$$

$$\Delta G = \Delta H - T\Delta S \quad (10)$$

where K_d represents the distribution coefficient, T is the absolute temperature (K) and R is the gas constant (8.314 J mol^{-1} K^{-1}). The plot of In K_d against 1/T (van' Hoff plot) was used for evaluating the values of ΔH and ΔS from the slope and intercept, respectively.

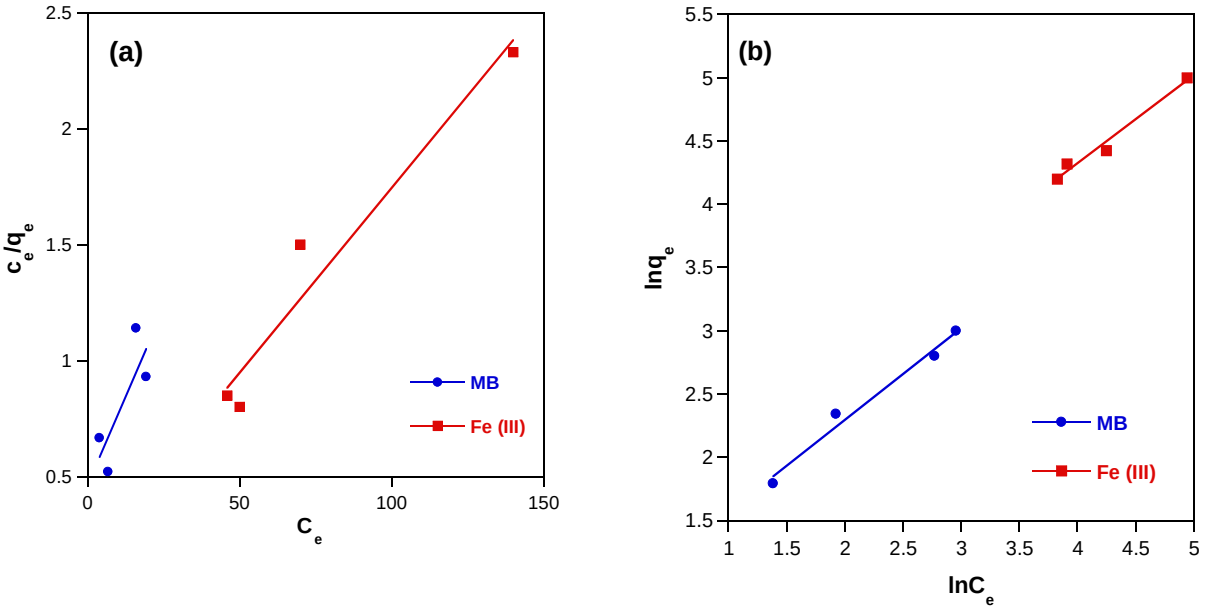

Fig. 8 Adsorption isotherm: (a) Langmuir isotherm, and (b) Freundlich isotherm.

The resultant straight lines for MB (R^2 = 0.984) and Fe (III) (R^2 = 0.973) are given in Figure 9. The values of ΔG at different temperatures were calculated from Eq. 10. The obtained thermodynamic parameters for the adsorption of MB and Fe (III) on $Ni(OH)_2$/PS composite are summarized in Table 3.

Table 3: The thermodynamic parameters for the adsorption of MB and Fe (III) on $Ni(OH)_2$/PS composite.

	ΔG (kJ mol^{-1})						
	303K	313K	323K	333K	343K	ΔH (kJ mol^{-1})	ΔS (J mol^{-1} K^{-1})
MB	-0.075	-0.415	-0.755	-1.095	-1.435	10.23	34.01
Fe (III)	-0.467	-0.737	-1.01	-1.278	-1.548	7.73	27.05

The positive values of ΔH confirmed that the adsorption processes were endothermic. This agrees with the favorability of the adsorption process observed when temperature was increased (Fig. 9a). The positive values of ΔS reveal that the adsorption processes involved an increase in randomness at the adsorbent/adsorbate interface. Besides, the negative values observed for ΔG indicates the feasibility and spontaneity of the adsorption processes as well as proved the good accessibility of the Ni(OH)2/PS composites toward MB and Fe(III). In addition, it seems that the adsorption processes were driven by the increment in entropy rather than enthalpy change.

4. Conclusions

In this research $Ni(OH)_2$/PS composites were prepared and tested as adsorbents for cationic species containing water including methylene blue dye and Fe (III). XRD, FT-IR and EDX analysis confirmed the structure of the composite. BET specific surface area measurements indicated the high area of the composite. Adsorption studies showed that contact time, composite dose and temperature positively increased the removal efficiency of MB and Fe (III) on the composite. By applying kinetic and isotherm models on the experimental data of adsorption, it was noted that the process followed the pseudo-first-order reactions and Freundlich isotherm. The thermodynamics studies revealed that the adsorption

was endothermic, however it was spontaneous and feasible (ΔG exhibited negative values). This means that the adsorption was driven by entropy change rather than enthalpy change.

5. Conflicts of interest

There are no conflicts to declare.

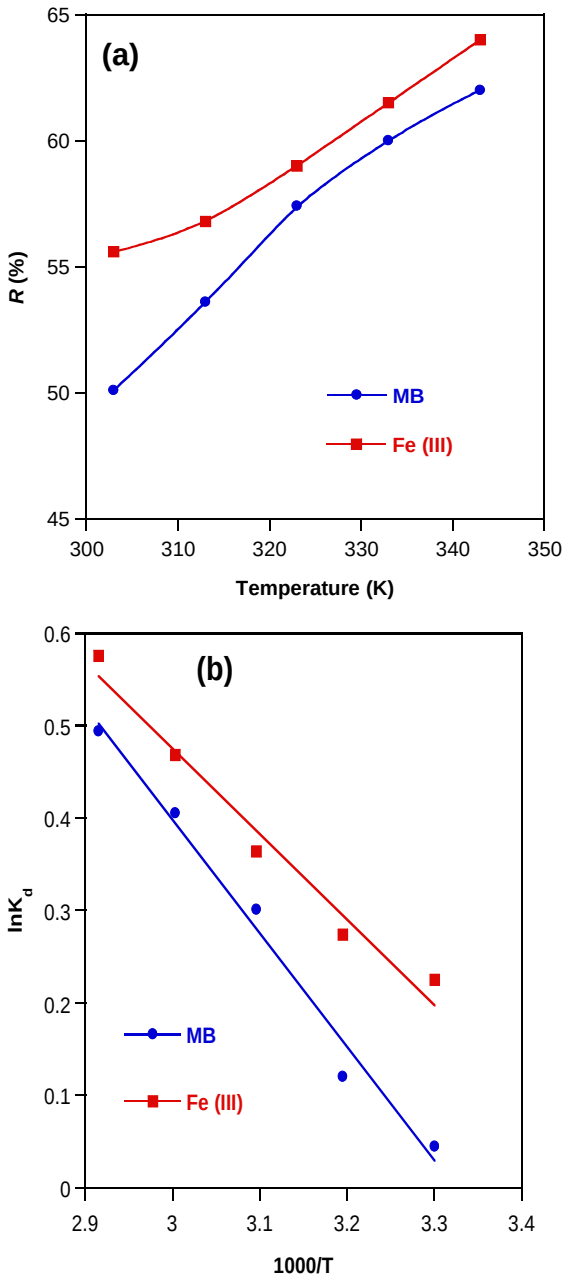

Fig. 9 (a) Influence of temperature on the adsorption of MB and Fe (III) on $Ni(OH)_2$/PS composites. (b) Plots of ln (K_d) versus (1000/T).

6. References

[1] W. S. Chai *et al.*, "A review on conventional and novel materials towards heavy metal adsorption in wastewater treatment application," *J. Clean. Prod.*, p. 126589, 2021.

[2] S. F. Mohsenpour, S. Hennige, N. Willoughby, A. Adeloye, and T. Gutierrez, "Integrating micro-algae into wastewater treatment: A review," *Sci. Total Environ.*, vol. 752, p. 142168, 2021.

[3] A. Saravanan *et al.*, "Effective water/wastewater treatment methodologies for toxic pollutants removal: Processes and applications towards sustainable development," *Chemosphere*, p. 130595, 2021.

[4] A. Bakry, M. S. A. Darwish, and T. F. Hassanein, "Adsorption of methylene blue from aqueous solutions using carboxyl/nitro-functionalized microparticles derived from polypropylene waste," *Iran. Polym. J.*, pp. 1–13, 2021, doi: 10.1007/s13726-021-00979-w.

[5] S. Khandaker, S. Das, M. T. Hossain, A. Islam, M. R. Miah, and M. R. Awual, "Sustainable approach for wastewater treatment using microbial fuel cells and green energy generation-A comprehensive review," *J. Mol. Liq.*, p. 117795, 2021.

[6] S. Jafarinejad, "Forward osmosis membrane technology for nutrient removal/recovery from wastewater: Recent advances, proposed designs, and future directions," *Chemosphere*, vol. 263, p. 128116, 2021.

[7] A. A. Elzoghby, A. Bakry, A. M. Masoud, W. S. Mohamed, M. H. Taha, and T. F. Hassanein, "Synthesis of polyamide-based nanocomposites using green-synthesized chromium and copper oxides nanoparticles for the sorption of uranium from aqueous solution," *J. Environ. Chem. Eng.*, vol. 9, no. 6, p. 106755, 2021, doi: 10.1016/j.jece.2021.106755.

[8] N. Udomkittayachai, W. Xue, K. Xiao, C. Visvanathan, and A. S. Tabucanon, "Electroconductive moving bed membrane bioreactor (EcMB-MBR) for single-step decentralized wastewater treatment: Performance, mechanisms, and cost," *Water Res.*, vol. 188, p. 116547, 2021.

[9] R. Huang, Q. Zhang, H. Yao, X. Lu, Q. Zhou, and D. Yan, "Ion-Exchange Resins for Efficient Removal of Colorants in Bis (hydroxyethyl) Terephthalate," *ACS omega*, vol. 6, no. 18, pp. 12351–12360, 2021.

[10] X. Xiao, Y. Yu, Y. Sun, X. Zheng, and A.

Chen, “Heavy metal removal from aqueous solutions by chitosan-based magnetic composite flocculants,” *J. Environ. Sci.*, vol. 108, pp. 22–32, 2021.

[11] A. S. Morshedy, M. H. Taha, D. M. Abd El-Aty, A. Bakry, and A. M. A. El Naggar, “Solid waste sub-driven acidic mesoporous activated carbon structures for efficient uranium capture through the treatment of industrial phosphoric acid,” *Environ. Technol. Innov.*, vol. 21, p. 101363, 2021, doi: https://doi.org/10.1016/j.eti.2021.101363.

[12] R. Rashid, I. Shafiq, P. Akhter, M. J. Iqbal, and M. Hussain, “A state-of-the-art review on wastewater treatment techniques : the effectiveness of adsorption method,” *Environ. Sci. Pollut. Res.*, vol. 28, pp. 9050–9066, 2021.

[13] C. R. Chandraiahgari, G. De Bellis, A. Martinelli, A. Bakry, A. Tamburrano, and M. S. Sarto, “Nanofiller induced electroactive phase formation in solution derived poly(vinylidene fluoride) polymer composites,” in *2015 IEEE 15th international conference on nanotechnology (IEEE-NANO)*, 2015, pp. 1346–1349, doi: 10.1109/NANO.2015.7388884.

[14] A. Bakry, M. S. A. Darwish, and A. M. A. El Naggar, “Assembling of hydrophilic and cytocompatible three-dimensional scaffolds based on aminolyzed poly(l-lactide) single crystals,” *New J. Chem.*, vol. 42, no. 20, pp. 16930–16939, 2018, doi: 10.1039/c8nj03205j.

[15] G. Casini *et al.*, “Functionalized poly(l-lactide) single crystals coated with antigens in development of vaccines.,” *J. Control. Release*, vol. 148, no. 1, pp. e105–e111, 2010, doi: 10.1016/j.jconrel.2010.07.080.

[16] A. Bakry *et al.*, “A new approach for the preparation of hydrophilic poly(L-lactide) porous scaffold for tissue engineering by using lamellar single crystals,” *Polym. Int.*, vol. 61, no. 7, pp. 1177–1185, 2012, doi: 10.1002/pi.4197.

[17] F. A. Morsy, S. Y. Elsayad, A. Bakry, and M. A. Eid, “Surface properties and printability of polypropylene film treated by an air dielectric barrier discharge plasma,” *Surf. Coatings Int. Part B Coatings Trans.*, vol. 89, no. 1, pp. 49–55, 2006, doi: 10.1007/BF02699614.

[18] A. Bakry, “Synergistic effects of surface grafting with heparin and addition of poly(d,l-lactide) microparticles on properties of poly(l-lactide) single crystals scaffolds,” *J. Appl. Polym. Sci.*, vol. 136, no. 30, pp. 47797-, 2019, doi: 10.1002/app.47797.

[19] A. Bakry, “Synergistic effects of surface aminolysis and hydrolysis on improving fibroblast cell colonization within poly (L-lactide) scaffolds,” *J. Appl. Polym. Sci.*, vol. 138, no. 1, p. 49643, 2020, doi: https://doi.org/10.1002/app.49643.

[20] A. Martinelli, A. Bakry, L. D’Ilario, I. Francolini, A. Piozzi, and V. Taresco, “Release behavior and antibiofilm activity of usnic acid-loaded carboxylated poly(l-lactide) microparticles,” *Eur. J. Pharm. Biopharm.*, vol. 88, no. 2, pp. 415–423, 2014, doi: 10.1016/j.ejpb.2014.06.002.

[21] B. Wang *et al.*, “Development of Nanocomposite Adsorbents for Heavy Metal Removal from Wastewater,” *ES Mater. Manuf.*, vol. 2, no. Vi, pp. 35–44, 2018, doi: 10.30919/esmm5f175.

[22] M. S. A. M. S. A. Darwish, A. Bakry, L. M. L. M. Al-Harbi, M. M. M. M. Khowdiary, A. A. A. El-Henawy, and J. Yoon, “Core/shell PA6@ Fe3O4 nanofibers: Magnetic and shielding behavior,” *J. Dispers. Sci. Technol.*, vol. 41, no. 11, pp. 1711–1719, 2020, doi: 10.1080/01932691.2019.1635025.

[23] M. S. A. M. S. A. Darwish, A. Bakry, O. Kolek, L. Martinová, and I. Stibor, “Electrospun functionalized magnetic polyamide 6 composite nanofiber: Fabrication and stabilization,” *Polym. Compos.*, vol. 40, no. 1, pp. 296–303, 2019, doi: 10.1002/pc.24647.

[24] M. R. Berber, “Current Advances of Polymer Composites for Water Treatment and Desalination,” *J. Chem.*, vol. 2020, 2020, doi: 10.1155/2020/7608423.

[25] D. T. Sun *et al.*, “Rapid, Selective Heavy Metal Removal from Water by a Metal-Organic Framework/Polydopamine Composite,” *ACS Cent. Sci.*, vol. 4, no. 3, pp. 349–356, 2018, doi: 10.1021/acscentsci.7b00605.

[26] H. Han, M. K. Rafiq, T. Zhou, R. Xu, O. Mašek, and X. Li, “A critical review of clay-based composites with enhanced adsorption performance for metal and organic pollutants,” *J. Hazard. Mater.*, vol. 369, pp. 780–796, 2019.

[27] H. Fan *et al.*, “Controllable Synthesis of Ultrathin Transition-Metal Hydroxide Nanosheets and their Extended Composite Nanostructures for Enhanced Catalytic Activity in the Heck Reaction,” *Angew. Chemie*, vol. 128, no. 6, pp. 2207–2210, 2016, doi: 10.1002/ange.201508939.

[28] F. Mohamed, M. R. Abukhadra, and M.

Shaban, "Removal of safranin dye from water using polypyrrole nanofiber/Zn-Fe layered double hydroxide nanocomposite (Ppy NF/Zn-Fe LDH) of enhanced adsorption and photocatalytic properties," *Sci. Total Environ.*, vol. 640, pp. 352–363, 2018.

[29] J. Fang, Y. Xuan, and Q. Li, "Preparation of polystyrene spheres in different particle sizes and assembly of the PS colloidal crystals," *Sci. China Technol. Sci.*, vol. 53, no. 11, pp. 3088–3093, 2010, doi: 10.1007/s11431-010-4110-5.

[30] M. Gao *et al.*, "Efficient water oxidation using nanostructured α-nickel-hydroxide as an electrocatalyst," *J. Am. Chem. Soc.*, vol. 136, no. 19, pp. 7077–7084, 2014, doi: 10.1021/ja502128j.

[31] K. S. W. S. S. J. Gregg, *Adsorption, Surface Area, and Porosity*, 2nd Editio. Academic Press, London, 1982.

[32] S. Netpradit, P. Thiravetyan, and S. Towprayoon, "Adsorption of three azo reactive dyes by metal hydroxide sludge: Effect of temperature, pH, and electrolytes," *J. Colloid Interface Sci.*, vol. 270, no. 2, pp. 255–261, 2004, doi: 10.1016/j.jcis.2003.08.073.

[33] S. K. Lagergren, "About the theory of so-called adsorption of soluble substances," *Sven. Vetenskapsakademiens Handl.*, vol. 24, pp. 1–39, 1898.

[34] Y. S. Ho and G. Mckay, "Pseudo-second order model for sorption processes," *Process Biochem.*, vol. 34, pp. 451–465, 1999.

[35] V. Vadivelan and K. V. Kumar, "Equilibrium , kinetics , mechanism , and process design for the sorption of methylene blue onto rice husk," *J. Colloid Interface Sci.*, vol. 286, no. 1, pp. 90–100, 2005, doi: 10.1016/j.jcis.2005.01.007.

[36] Y. S. Won, S.W., Vijayaraghavan, K., Mao, J., Kim, S. and Yun, "Reinforcement of carboxyl groups in the surface of Corynebacterium glutamicum biomass for effective removal of basic dyes," *Bioresour. Technol.*, vol. 100, no. 24, pp. 6301–6306, 2009.